Indian Journal of Chemistry
Vol. 61, April 2022, pp. 370-384

SAR-based approach to explore in silico ferrocene analogues as the potential inhibitors of major viral proteins of SARS-CoV-2 virus and human Ca^{2+}-channel blocker

Maynak Pal[a], Dulal Musib[a] & Mithun Roy[a,] *

Department of Chemistry, National Institute of Technology Manipur, Langol 795 004, Manipur, India

*E-mail: mithunroy@nitmanipur.ac.in

Received 09 November 2021; revised and accepted 28 March 2022

Amid the pandemic COVID-19, there is a desperate and urgent need for a therapeutic solution for COVID-19. Our present studies have adapted the SAR-based approach to explore in silico several selected ferrocene-based complexes as the potential inhibitors of the major viral proteins (Spike, RdRp, M_{pro}, N protein) of the SARS-CoV-2 virus. The SAR-based molecular docking studies have revealed that compound 1 is the strongest inhibitor of the major viral proteins with a binding energy of >9.0 kcal/mol. Compound 1 is also able to inhibit the human Ca^{2+} channel and thereby potentially able to prevent the strong inflammatory signalling cascades causing severe respiratory distress to the COVID-19 patients. Overall, our computational studies explored ferrocene-based compounds as the emerging multi-targeting therapeutic solution for COVID-19 by inhibiting viral replication as well as modulating the inflammatory signalling cascades.

Keywords: COVID-19, Ferrocene based complexes, Spike protein, RdRp protein, M_{pro} protein and N protein inhibitors, Human Ca^{2+}-channel blocker

The pandemic COVID-19, caused by the outbreak of SARS-CoV-2 virus resulted in the greatest global health crisis of the present century. The pandemic resulted in 188 million infections along with 4.0 million morbidities till now since November 2019 across the globe[1]. The virus SARS-CoV-2 was a novel mutant virus of the variant SARS-CoV and MERS that were broken out in 2003 and 2012, respectively. SARS-CoV and MERS viruses were although more fatal, but less transmittable, and limited to less than a few thousand cases across the world.[2-4] The severity of the SARS-CoV-2 virus was caused due to the higher transmutability of the virus through respiratory droplets. The virus eventually settles in the nasal tract and follows the way to the lungs, where the virus primarily interacts with the ACE2 receptors of the alveolar epithelial cells through the spike protein trimers. The viral RNA genome then enters the host cells and further gets translated and replicated in the host cells using the host cell's machinery. This eventually leads to the formation of new progeny virions with the help of several membrane proteins of the virus such as nucleocapsid (N) protein, envelope (E) protein, and membrane (M) protein, and many non-structural proteins.[5-7]

Prevention of the spread of the virus and death toll became a primary objective so far. Social distancing and frequent sanitization had prevented the spread of the corona virus to some extent.[8] Several spike protein and RNA-based vaccines, developed recently, were now rolling across the globe which could prevent viral infections and reduces the severity of the viral outbreak.[9-12] The emergence of several mutant strains of SARS-CoV-2 virus in early 2021 severely affected the efficacy of the vaccines and resulted in several waves of the viral outbreak.[13-15]

Due to the dire need for therapy for COVID-19, the World Health Organization (WHO) had recommended repurposing of current FDA-approved antiviral drugs like hydroxychloroquine, remdesivir, arbidol, ribavirin, nelfinavir, baloxavir, favipiravir, methisazone, tenofovir, lopinavir/ritonavir/ribavirin for the treatment of COVID-19 patients.[16-18] Several anticancer drugs like geftinib were also repurposed for the treatment of COVID-19.[19] The efficacy of the repurposed drug was highly dependent on the specific strains of the SARS-CoV-2 virus and there was a failure of choice of the proper drug against COVID-19. Moreover, the repurposed antiviral drugs were often associated with severe side effects and were

withdrawn from the therapeutic protocol for COVID-19.[20-21] Therefore, finding a proper therapeutic solution for the COVID-19 was the dire need of the hour.

Structural and molecular biology of the SARS-CoV-2 virus was revealed with almost a minute detail and molecular understanding of the virus offer us ample scope to design a drug for COVID-19. There were four main structural protein of SARS-CoV-2 virus *e.g.* spike (S) protein, nucleocapsid (N) protein, envelope (E) protein, and membrane (M) protein. The spike protein consists of three trimeric protein units and each unit contains two subunits like S1 and S2. The S1 subunit contains the most vital receptor binding domain (RBD) and is responsible for the recognition and binding to the ACE2 receptor strongly following the viral entry into the host alveolar epithelial cells.[22] Transcription and translation of the viral RNA genome and following complex biochemical processes involving RNA-dependent RNA polymerase (RdRp) and proteolytic cleavage in proteins in several structural and non-structural proteins, the viral replication was taking place in the host cells.[23] The envelope (E) protein plays a major role in the virus morphogenesis and assembly. It also acts as viroporin and it was capable of self-accumulating in host membranes.[24] The self-assembly in the host membrane was the reason for the formation of pentameric protein-lipid pores which were responsible for ion transport.[25] The membrane (M) protein was responsible for the binding of all supplementary structural proteins during the formation of new progeny virions.[26] The drug interacting strongly with the key viral proteins like Spike protein, RdRp, M_{pro}, M or E-protein could offer a therapeutic solution against SARS-CoV-2 virus, that inhibit viral replication processes (Fig. 1).

Acute respiratory distress syndrome (ARDS) in the COVID-19 patients resulted in hypoxia which is reported to cause the alteration of the cell calcium dynamics and results in the alterations to several signal transduction pathways and gene expression. Recently it is reported that both viruses and hypoxia directly modulate several pathological and biochemical pathways like inflammation, glycolysis, cytokine signalling, and calcium signalling.[27-29] Therefore, blocking or modulating the Ca^{2+}-channel that inhibit could be an attractive strategy to prevent hyper-inflammation and ARDS outcome (Fig. 1).

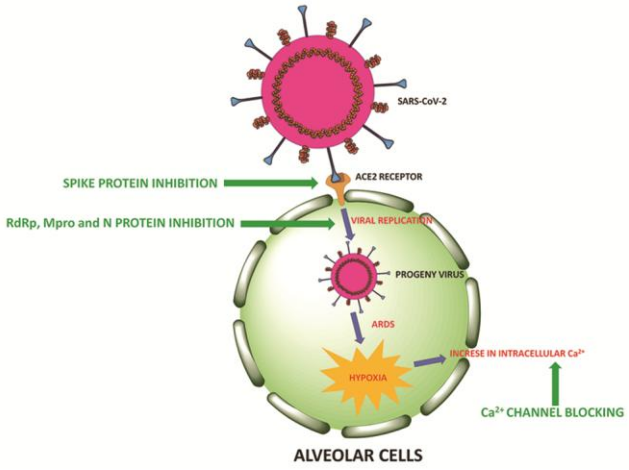

Fig. 1 — Schematic representation of SARS-CoV-2 infection of the alveolar cells (red) and their prevention strategies (green)

Sustainable synthesis and derivatization of ferrocenyl compounds due to their remarkable air and aqueous stability, tunable redox chemistry, lipophilicity and enhanced cellular permeability of ferrocenyl compounds had emerged as the viable tools for medicinal applications.[30-32] Antimalarial ferroquine and anticancer ferrocifen were the only ferrocenyl organometallic compounds under the clinical trials.[33] Several other ferrocenyl compounds were potentially explored for anticancer, antiparasitic, antibacterial, and antiviral applications.[34-35] Moreover, the Fe^{2+}center in ferrocene could play a vital role in coordinating with the N-containing amino acid residues of proteins resulting in additional stabilization of drug-protein complex and reflected in binding energy.[36]

Recently in silico drugs design plays a major role in drug development.[37-38] Molecular docking was one of the powerful tools to explore the binding efficacy of the drug with its target protein and provide in-depth detail of the interactions between the drugs and the associated proteins in its binding pocket. We had recently demonstrated the sustainable utility of transition metal complexes including ferrocene-based compounds against the SARS-CoV-2 virus by inhibiting the key viral proteins.[36] The high binding affinity of ferrocenyl compounds with RdRp of SARS-CoV-2 virus had prompted us to explore binding efficacy in silico of the several ferrocenyl compounds with the different key viral proteins of SARS-CoV-2 virus in a SAR-based approach. Here in, we had reported the structure activity relationship of the FDA approved drugs Ferroquine, Ferrocifen,

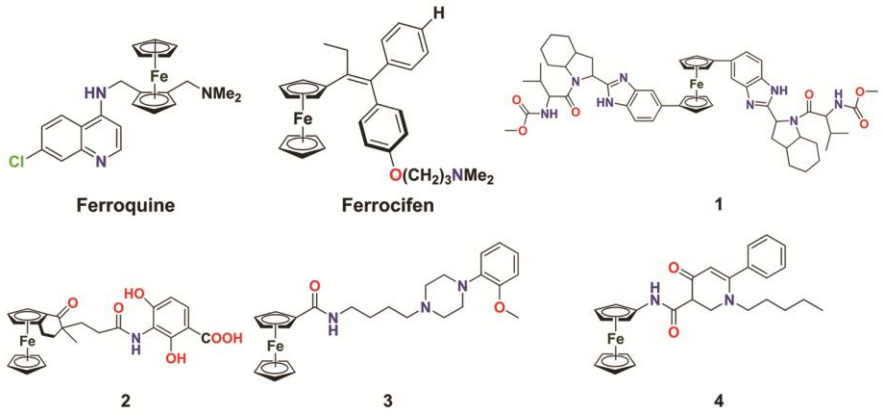

Scheme 1 — Selected ferrocene-based compounds for molecular docking studies against major viral proteins of SARS-CoV-2

and several other ferrocene Compounds on interacting with the key viral proteins of SARS-CoV-2 (Scheme 1, Table 1).

Experimental Details

We had selected Ferroquine, Ferrocifen, and four other antiviral and anticancer ferrocene compounds for molecular docking with the main structural proteins of SARS-CoV-2. These proteins were spike protein (PDB Id: 6VXX), RNA dependent RNA polymerase, RdRp protein (PDB Id: 6M71), nucleocapsid protein (PDB Id: 6M3M), and main protease (PDB Id: 6LU7). The crystal structures of the protein structures were obtained from the Protein Data Bank (PDB) database as .pdb format.[39-42] Prior to the molecular docking studies, the proteins were prepared by deleting the water molecules and auxiliary ligand and followed by the addition of polar hydrogens and the addition of Gestiger charges. The geometry optimized structures of the complexes were used for molecular docking. The geometry optimization was performed using the LAN2DZ basis set in Gaussian 09 software [43]. Prior to any further studies, the ADME analysis of the compounds was carried out to get a conclusive idea of their pharmacokinetics and understanding of their acceptability as drugs [44]. Molecular docking was performed using Autodock 4 software [45]. The binding sites were identified for each protein and the molecular docking grid was prepared accordingly (Table S1). The molecular docking was performed considering the pH media 7 and the docking parameters were set to long (250000000) along with keeping other parameters as default. The output file was saved in Lamarckian GA format. The output files contain the binding parameters. The docked poses were analysed for interactions with the proteins using Discovery Studio 9 software [46].

Table 1 — Medicinal properties of selected metal complexes

Name of the compound	Medicinal properties	Reference
Ferroquine	FDA approved antimalarial drug. It also possesses anti-bacterial and anticancer activities	36
Ferrocifen	Highly active against breast cancer cells, targets thioredoxin reductase (TrxR), Glutathione reductase	34
1	inhibit the HSV protein with inhibition constant EC_{50} value 15 pM,	36
2	Ferrocenyl analogue of the drug BP 897 that exhibits higher lipophilicity than its organic congener and targets human cannabinoid receptors CB1 and CB2, the two subclasses of an important family of GPCRs	34
3	Ferrocenyl analogue of the drug BP 897 that exhibits higher lipophilicity than its organic congener and targets human cannabinoid receptors CB1 and CB2, the two subclasses of an important family of GPCRs	34
4	Ferrocenyl analogue of the drug BP 897 that exhibits higher lipophilicity than its organic congener and targets human cannabinoid receptors CB1 and CB2, the two subclasses of an important family of GPCRs	34

Results and Discussion

Ferroquine as the inhibitor of major proteins of SARS-CoV-2

In the last few decades ferrocene-based compounds had emerged as a potential tool for medicinal for antitumor, antimalarial, anti-HIV and antibacterial applications. Ferroquine was in phase III clinical trial as an antimalarial agent and exhibited better efficacy than chloroquine or hydroxychloroquine. Herein, we explored the potential repurposing of ferroquine against SARS-CoV-2 virus. Ferroquine contains five rotatable bonds with three hydrogen bond acceptor

atoms and two hydrogen bond donor atoms with a total polar surface area of 27.30 $Å^2$. These characteristics make ferroquine suitable for inhibition of the viral proteins via the formation of several noncovalent bond with the amino acid residues of the proteins. The ADME analysis revealed that ferroquine had a consensus Log $P_{o/w}$ of 2.36 and it was moderately soluble in water. It also had high gastrointestinal absorption and blood brain barrier permeability with an additional property to inhibit CYP3A4 protein. The ADME analysis also predicted ferroquine to be used as an oral or intravenous drug. The drug-likeness analysis revealed zero violations in terms of Lipinsky, Ghose, Veber, Egan, Muegge analysis suggest the acceptability of ferroquine as a drug. We previously had reported the efficacy of ferroquine towards the inhibition of spike protein and RdRp of SARS-CoV-2 with binding energies of -7.43 kcal/mol and -6.19 kcal/mol, respectively. In our present work, we explored further in the binding affinity of ferroquine towards other key viral proteins $M_{pro}$and N-protein SARS-CoV-2 virus. The molecular docking of ferroquine in the M_{pro} of SARS-CoV-2 resulted in the binding energy of -9.28 kcal/mol with an inhibition constant of 0.15725 μM (Fig. S1, Table 2, 3). This binding energy was attributed to the

Table 2 — The probable binding parameters between the selected compounds and major viral proteins of SARS-CoV-2 and compound 1 with human Ca^{2+} channel protein

Compound [a]	Protein	Binding Energy [b] [c]	Inhibition Constant [d]	Intermolecular Energy [b]	Vdw Hb Dissolution Energy [b]	Electrostatic Energy [b]	Total Internal [b]	Torsional Energy [b]
Ferroquine[e]	Spike	-7.43	3.56	-9.08	-7.12	0.08	-1.31	1.79
Ferroquine[f]	RdRp	-6.19	28.88	-8.58	-7.06	-1.52	-1.05	2.39
Ferroquine	M_{pro}	-9.28	0.15725	-11.07	-9.97	-1.1	-1.09	1.79
Ferroquine	N	-6.91	8.61	-8.7	-8.76	0.06	-1.27	1.79
Ferrocifen	Spike	-5.89	48.26	-8.87	-8.09	-0.79	-2.43	2.98
Ferrocifen	RdRp	-6.81	10.19	-9.79	-9.31	-0.48	-2.68	2.98
Ferrocifen	M_{pro}	-8.69	0.4299	-11.67	-11.19	-0.48	-2.25	2.98
Ferrocifen	N	-7.09	6.4	-10.07	-10.08	0.01	-1.91	2.98
1	Spike	-9.62	0.08854	-13.8	-13.55	-0.25	-5.01	4.18
1	RdRp	-9.42	0.12363	-13.6	-13.28	-0.32	-6.21	4.18
1	M_{pro}	-13.12	0.002398	-17.3	-16.76	-0.54	-5.38	4.18
1	N	-8.88	0.31102	-11.56	-10	-1.57	-3.35	4.18
1	Human Ca^{2+} channel	-13.74	0.000085	-17.61	-17.59	-0.02	-5.13	4.18
2	Spike	-6.67	12.94	-9.35	-9.42	0.07	-2.77	2.68
2	RdRp	-6.84	9.66	-9.53	-7.12	-2.41	-3.13	2.68
2	M_{pro}	-10.18	0.03472	-12.86	-11.23	-1.63	-2.98	2.68
2	N	-7.99	1.38	-10.68	-10.18	-0.5	-3.01	2.68
3	Spike	-9.38	0.13308	-11.47	-8.37	-3.1	-0.7	2.09
3	RdRp	-8.91	0.29582	-11	-9.24	-1.76	-0.94	2.09
3	M_{pro}	-10.15	0.035	-12.24	-10.71	-1.53	-0.71	2.09
3	N	-7.14	5.87	-9.22	-9.88	0.65	-0.71	2.09
4	Spike	-7.09	6.4	-9.17	-9.27	0.1	-0.77	2.09
4	RdRp	-8.59	0.50219	-10.68	-10.7	0.02	-0.52	2.09
4	M_{pro}	-9.46	0.11622	-11.55	-11.18	-0.37	-0.53	2.09
4	N	-7.92	1.57	-10.01	-9.94	-0.07	-1	2.09

[a] [The table contains the details of the interactions between the selected compounds and major viral proteins of SARS-CoV-2)

[b] [The energy values reported in the table contains the unit of kcal/mol.]

[c] [The binding energy value reported in the table corresponds to the binding free energy (ΔG) of the complex and spike glycol-protein. The other auxiliary factors contribute to the binding energy.]

[d] [The inhibition constant values are theoretically obtained and reported in the unit of μM]

[e] [This row indicates the details of interactions between Ferroquine and spike protein. The details are published in: M. Pal, D. Musib, A. J. Zade, N. Chowdhury, M. Roy, ChemistrySelect. 2021, 6, 7429-7435. DOI: 10.1002/slct.202101852]

[f] [This row indicates the details of interactions between Ferroquine and spike protein. The details are published in: M. Pal, D. Musib, M. Roy, New J. Chem. 2021, 45, 1924-1933. DOI: 10.1039/D0NJ04578K.]

[g] [This row indicates the details of interactions between compound 1 and human Ca^{2+} channel protein.

Table 3 — Competitive results of binding energy of the selected complexes with the proteins and the details of the interactions

Compound [a]	Protein	Binding energy [b],[c]	Inhibition constant [d]	Hydrogen bonds	Protein residue involved in formation of hydrogen bonding	Non covalent interactions	Protein residue involved in formation of non covalent bonding	Total number of bonds
Ferroquine[e]	spike	-7.43	3.56					
Ferrocifen	spike	-5.89	48.26	2	TYR421, ASP30.	5	ASP30, VAL417, HIS34, ARG393	7
1	Spike	-9.62	0.08854	6	GLN325, ARG408, GLN409	11	VAL417, ALA386, ALA387, VAL503, THR 324	17
2	Spike	-6.67	12.94	8	ARG393, GLY354, TYR505, ASP405, ALA386	6	ILE548, PRO620, ALA386, HIS34, ARG393	14
3	Spike	-9.38	0.13308	4	GLN76, GLU35, GLU75	-	-	4
4	Spike	-7.09	6.4	5	HIS34, ASN33, GLU37	3	LYS353, LYS403	8
Ferroquine[f]	RdRp	-6.19	28.88					
Ferrocifen	RdRp	-6.81	10.19	1	GLU436	5	LYS438, LYS43, LYS7, MET3, SER1	6
1	RdRp	-9.42	0.12363	6	LYS621, SER814, GLN815, ARG836, ASP865	7	ILE548, PRO620, LYS551, ALA550, ARG555	13
2	RdRp	-6.84	9.66	10	ARG553, LYS545, ARG553, ARG555, LYS621, CYS622, ASP623	2	ARG555, ARG553	12
3	RdRp	-8.91	0.29582	3	THR801, GLU802	2	TRP800, HIS810	5
4	RdRp	-8.59	0.50219	3	LEU473, PHE429, SER4	10	LEU437, LYS7, LYS438, CYS8, PHE440, PHE843, SER1	13
Ferroquine	M_{pro}	-9.28	0.15725	5	GLN127, GLN288, ASP289	4	LYS5	9
Ferrocifen	M_{pro}	-8.69	0.4299	5	GLN127, LYS137,	3	LYS5, ARG4	8
1	M_{pro}	-13.12	0.002398	7	LYS5, GLU288, LYS137	13	LEU282, GLY283, LYS5, ARG4	20
2	M_{pro}	-10.18	0.03472	7	LYS5, ARG4, GLN127	3	LYS5	10
3	M_{pro}	-10.15	0.035	7	LYS173, LEU287, ASP289, LEU287, ALA285,	7	MET276, LEU287, LEU272, LYS5, LYS137	14
4	M_{pro}	-9.46	0.11622	7	LYS5, GLN127, SER4	4	LEU5, LYS5	11
Ferroquine	N	-6.91	8.61	4	THR149, ALA156, ILE75, VAL159	5	ALA156, ILE158, TRP53, ILE158	9
Ferrocifen	N	-7.09	6.4	3	ASN76, SER79, THR77	3	LYS5, PRO163, LEU168	6
1	N	-8.88	0.31102	6	GLN164, GLN 161, LEU168, LYS170, GLN71	5	LEU160, LEU162, LEU168, PRO163	11
2	N	-7.99	1.38	8	GLU137, GLN161, LEU162, GLY165, THR166, GLY70	1	LEU162	9
3	N	-7.14	5.87	3	GLN71, GLN84, GLY70	3	LEU160, LEU162, LEU 168	6
4	N	-7.92	1.57	4	GLU137, THR166	2	PRO163, LEU168	6
1	human Ca^{2+}-channel protein	-13.74	0.	7	LYS1462, ASN952, MET1508, THR921, ASN388	5	ILE387, VAL1339, MET1508, LEU1813	12

[a] [The table contains the details of the interactions between the selected compounds and major viral proteins of SARS-CoV-2)

[b] [The energy values reported in the table contains the unit of kcal/mol.]

[c] [The binding energy value reported in the table corresponds to the binding free energy (ΔG) of the complex and spike glycol-protein. The other auxiliary factors contribute to the binding energy.]

[d] [The inhibition constant values are theoretically obtained and reported in the unit of μM]

[e] [This row indicates the details of interactions between Ferroquine and spike protein. The details are published in: M. Pal, D. Musib, A. J. Zade, N. Chowdhury, M. Roy, ChemistrySelect. 2021, 6, 7429-7435. DOI: 10.1002/slct.202101852]

[f] [This row indicates the details of interactions between Ferroquine and spike protein. The details are published in: M. Pal, D. Musib, M. Roy, New J. Chem. 2021, 45, 1924-1933. DOI: 10.1039/D0NJ04578K.]

formation of several noncovalent interactions as follows-

(i) Two hydrogen bonds with the GLN127 residue of protein where ferroquine acts as donor and O atoms of the residue acts as acceptors.
(ii) Three carbon-hydrogen bonds with the GLN288, ASP289 residue of protein where ferroquine acts as donor and O atoms of respective residues act as acceptors.
(iii) One hydrophobic alkyl-alkyl interaction with the LYS5 residue.
(iv) One hydrophobic π-alkyl interaction with the LYS5 residue.
(v) Two electrostatic attractive interactions with the LYS5 N atom and the Fe^{2+}center with an effective distance of 5.2298 and 5.26713 Å respectively. Such interactions had a remarkable effect on the binding of ferroquine to the M_{pro} with the contribution of -9.28 kcal/mol.

Ferroquine also inhibits the N-protein of SARS-CoV-2 resulting in the binding energy of -6.91 kcal/mol with an inhibition constant of 8.61. µM (Fig. S2, Table 2, 3). This binding energy was attributed to the formation of several noncovalent interactions as followed-

(i) Two hydrogen bonds with the THR149, ALA156 residue of protein where ferroquine acts as donor and O atoms of the residue acts as acceptors.
(ii) Two carbon-hydrogen bonds with the ILE75, VAL159 residue of protein where ferroquine acts as donor and O atoms of respective residues acts as acceptors.
(iii) Two hydrophobic alkyl-alkyl interactions with the ALA156, ILE158 residue.
(iv) One hydrophobic π-alkyl interaction with the TRP53 residue.
(v) Two hydrophobic π-σ interactions with the TRP53, ILE158 residue.

The overall results indicated that ferroquine was able to inhibit major viral proteins of SARS-CoV-2 virus with better efficacy in many of cases due to the involvement of Fe^{2+} in interacting with the amino acid residues of the protein.

Ferrocifen as the inhibitor of major proteins of SARS-CoV-2

Ferrocifen is another ferrocenyl organometallic compound that had been reported for its antitumor activities and it was under preclinical trial. Ferrocifen having major structural similarities with ferroquine, can also exhibit inhibition of the main viral proteins of SARS-CoV-2 virus. Ferrocifen contains nine rotatable bonds with two hydrogen bond acceptor atoms with a total polar surface area of 12.47 $Å^2$. Hence ferrocifen can attain a suitable structural orientation for maximizing of inhibition of the viral proteins via the formation of several noncovalent bond with the amino acid residues of the proteins. But due to the lack of hydrogen bond acceptors, the inhibition efficacy of ferrocifen was expected to be less than that of ferroquine. The ADME analysis reveals, ferrocifen had a consensus $LogP_{o/w}$ of 5.11 and it was weakly soluble in water. It had low gastrointestinal absorption and blood brain barrier permeability with an additional property to inhibit CYP3A4 protein. This indicates the application of ferrocifen as an intramuscular drug. The drug likeness analysis reveals a couple of violations in terms Lipinsky, Ghose, Veber, Egan, Muegge analysis. These were mainly because of the low solubility of the compound in water. By using it as an intramuscular drug this was issue can be accounted for. It also attains zero PAINS alert and it was likely to be used as an intramuscular drug.

The molecular docking data reveals that ferrocifen had an ability to inhibit the spike protein of SARS-CoV-2 with a binding constant of -5.89 kcal/mol and an inhibition constant of 48.26 µM (Fig. S3, Table 2, 3). The binding energy was attributed for the following noncovalent interactions-

(i) Two carbon-hydrogen bonds with the TYR421 and ASP30 residue of protein where ferrocifen acts as donor and O atoms of the residue acts as acceptors.
(ii) One electrostatic π-anion interaction with the ASP30 residue.
(iii) Two hydrophobic π-alkyl interactions with the VAL417 residue.
(iv) Two electrostatic attractive interactions with the HIS34 and ARG393 N atoms and Fe^{2+}center with an effective distance of 4.85182 and 5.14439 Å, respectively.

The binding constant value was not high due to the lack of hydrogen bonds acceptors but was comparable to several repurposed antiviral drugs used for COVID-19.

Ferrocifen interacts with the RdRp protein with the binding energy of -6.81 kcal/mol and inhibition

constant of 10.19 μM (Fig. S4, Table 2, 3), resulted from the following molecular interactions.

(i) One hydrogen bond with the GLU436 residue of protein where ferrocifen acts as donor and O atoms of the residue acts as acceptor.
(ii) Four hydrophobic π-alkyl interactions with the LYS438, LYS43, LYS7, MET3, residues.
(iii) One electrostatic attractive interaction with the SER1 N atom and the Fe^{2+}center with an effective distance of 3.92259 Å.

In spite of the lack of hydrogen bonds acceptors in ferrocifen, it exhibits decent binding efficacy to RdRp which was a key protein complex during the replication, transcription, and translation of viral RNA in the host cells.

Main protease (M_{pro}), which was another key viral protein responsible for viral replication, was also inhibited by ferrocifen. The binding energy and the inhibition constant determined from molecular docking studies were -8.69 kcal/mol and 0.4299 μM, respectively (Fig. S5, Table 2, 3). The molecular interactions attributing to the high binding affinity of ferrocifen to M_{pro} were

(i) Five carbon-hydrogen bonds with the GLN127, LYS137 residue of protein where ferrocifen acts as donor and O atoms of respective residues act as acceptors.
(ii) One hydrophobic π-alkyl interaction with the LYS5 residue.
(iii) Two electrostatic attractive interactions with LYS5 and ARG4 N atoms and Fe^{2+}center with an effective distance of 5.2389 and 5.39863 Å respectively.

Ferrocifen also can inhibit the N-protein of SARS-CoV-2 via the formation of several noncovalent interactions leading to the binding energy of -7.09 kcal/mol with an inhibition constant of 6.4 μM (Fig. S6, Table 2, 3). The observed molecular interactions were

(i) Three carbon-hydrogen bonds with the ASN76, SER79, THR77 residue of protein where ferrocifen acts as donor and O atoms of respective residues acts as acceptors.
(ii) One hydrophobic alkyl-alkyl interaction with the LYS5 residue.
(iii) Two hydrophobic π-alkyl interactions with the PRO163, LEU168 residues.

In this case the lack of formation of electrostatic interactions involving Fe^{2+} leads to moderate binding energy.

Overall, the lack of electrostatic interactions between Fe^{2+} and the amino acid residue of viral proteins become pivotal in explaining less binding efficacy of ferrocifen to the key viral proteins of SARS-CoV-2 virus. The binding energies were comparable to that of the repurposed FDA-approved antiviral drugs.

Compound 1 as the inhibitor of major proteins of SARS-CoV-2

The ferrocenyl compound **1** was reported to exhibit antitumor and antiviral activities and thus had prompted us to select **1** for in silico screening against SARS-CoV-2. The compound **1** consists of sixteen rotatable bonds with sixteen hydrogen bond acceptor atoms and eight hydrogen bond donor atoms with a total polar surface area of 167.11 $Å^2$. Hence the compound **1** could attain a proper orientation and enable compound **1** to form several noncovalent bonds with the amino acid residues of the proteins and indicated the potential of compound **1** to become a drug candidate against SARS-CoV-2. The ADME analysis reveals that compound **1** had a consensus Log $P_{o/w}$ of 5.44 and it was poorly soluble in water. It also had low gastrointestinal absorption and blood brain barrier permeability but it had an additional property to inhibit CYP3A4 protein. Therefore, the compound could be an intramuscularly administered drug. The drug likeness analysis reveals two violations in terms Lipinsky, Ghose, Veber, Egan, Muegge analysis due to its larger size and poor aqueous solubility.

Due to high polar surface area, high flexibility and a good amount of hydrogen bond donors and acceptors, compound **1** can exhibit a very high binding affinity towards the several viral proteins of SARS-CoV-2. It binds with the spike protein with a binding energy of -9.62 kcal/mol and an inhibition constant of 0.08854 μM (Fig. S7, Table 2, 3). The strong binding of compound 1 with the spike protein was attributable to the following noncovalent interactions.

(i) Six hydrogen bonds with the GLN325, ARG408, GLN409 residues of protein where compound **1** acts as acceptor and the residue acts as donors.
(ii) One hydrogen bond with the VAL417 residue of protein where compound **1** acts as a donor and N atom of residue acts as acceptor.
(iii) One π-donor hydrogen bond with the VAL417 residue of protein where compound **1** acts as acceptor and the residue act as a donor.

(iv) Two hydrophobic alkyl-alkyl interactions with the ALA386 and ALA387 residues.
(v) Two hydrophobic π-alkyl interactions with the VAL503, ALA386 residues.
(vi) Three hydrophobic π-σ interactions with the THR324, VAL503 residues.
(vii) Two hydrophobic π- π stacking interactions.

Due to the larger size of the compound **1,** it was very hard for Fe^{2+} to be involved in electrostatic interactions with the protein side chain amino acid residues. However, this was compensated by a large number of hydrogen bonding and other noncovalent interactions.

The compound **1** strongly interacts with the RdRp protein of SARS-CoV-2 with the binding energy of -9.42 kcal/mol and an inhibition constant of 0.12363 μM (Fig. S8, Table 2, 3). The molecular interactions attributed to such strong binding affinity were

(i) Four hydrogen bonds with the LYS621, SER814, GLN815, ARG836 residues of protein where the compound **1** acts as donor and O, S, N atoms of the residue acts as acceptors.
(ii) Two carbon-hydrogen bonds with the ASP865 residue of protein where the ferrocenyl compound **1** acts as donor and O atoms of respective residues acts as acceptors.
(iii) Two hydrophobic alkyl-alkyl interactions with the ILE548, PRO620 residues.
(iv) Three hydrophobic π-alkyl interactions with the LYS551, ALA550 residues.
(v) One hydrophobic π- π stacking interaction.
(vi) Two hydrophobic π-cationic interactions with LYS551, ARG555 residues.
(vii) Three electrostatic attractive interactions with the LYS551, ARG553, ARG555 residues N-atom and the Fe^{2+}center with an effective distance of 5.54317, 5.46952, and 5.18902 Å respectively.

Due to the hollow binding site provided by the RdRp protein, the compound **1** can bind with the protein via several electrostatic attractive interactions, but it also results in less exposure of complex with the amino acid residues which leads to the lesser number of hydrogen bonds in RdRp than that of the spike protein. Hence the binding energy was though quite high for RdRp but less than the spike protein.

The compound **1** most strongly binds with the Main protease (M_{pro}) of SARS-CoV-2, resulting in the binding energy of -13.12 kcal/mol with an inhibition constant of 0.0022398 μM (Fig. 2, Table 2, 3). The interactions that attribute to the high binding energy were as follows

(i) Two hydrogen bonds with the LYS5 residues of protein where the compound **1** acts as acceptor and the residue acts as donors.
(ii) Five hydrogen bonds with the GLU288, LYS137 residues of protein where compound **1** acts as a donor and O atom of residue acts as acceptor.

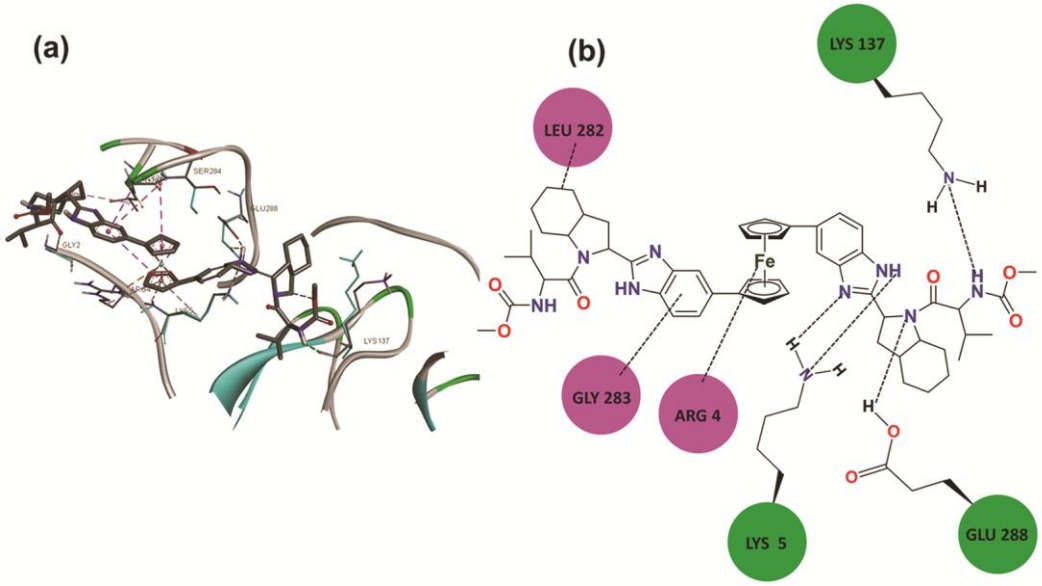

Fig. 2 — The best dock pose exhibiting non-covalent interactions between the compound **1** and the M_{pro} protein of SARS-CoV-2 and (b) Schematic representation of showing all the non-covalent interactions with LEU282, GLY283, ARG4, LYS5, GLU288, LYS137 residues

(iii) One π-donor hydrogen bond with the LYS5 residue of protein where the compound **1** acts as acceptor and the residue act as a donor.
(iv) Three carbon-hydrogen bonds with the GLY2 residue of protein where compound **1** acts as donor and O atoms of respective residues acts as acceptors.
(v) One hydrophobic alkyl-alkyl interaction with the LEU282 residue.
(vi) One hydrophobic π-σ interaction with the GLY283 residue.
(vii) Two hydrophobic π- π stacking interaction.
(viii) Two hydrophobic amide- π interaction with GLY283 residue.
(ix) Two hydrophobic π-alkyl interactions with LYS5, ARG4 residues.
(x) One electrostatic attractive interaction with the ARG4 residue N atom and the Fe^{2+}center with effective distance of 4.16037 Å.

The lateral shape of the binding site of the M_{pro} protein provides space for all of the molecular interactions and thereby the complex **1** can form three types of hydrogen bonds with a total of eight H-bonds and several other noncovalent interactions with one electrostatic attractive interaction by Fe^{2+}center. All these factors contribute to a very high binding energy in this case.

The binding propensity of the compound **1** to the N-protein was also explored through molecular docking studies. The docking studies revealed that the compound **1** binds strongly with the N-protein of SARS-CoV-2 with the binding energy of -8.88 kcal/mol and inhibition constant of 0.31102 μM (Fig. S9, Table 2, 3). The primary intermolecular interactions observed in the best docked pose were

(i) Four hydrogen bonds with the GLN164, GLN 161, LEU168, LYS170 residues of protein where compound **1** acts as acceptor and the residue acts as donors.
(ii) One hydrogen bond with the GLN164 residue of protein where compound **1** acts as a donor and O atom of the residue acts as acceptor.
(iii) One π-hydrogen bond with the GLN71 residue of protein where compound **1** acts as a donor and the residue act as an acceptor.
(iv) One hydrophobic π -σ interaction with the THR167 residue.
(v) Four hydrophobic π-alkyl interactions with the LEU160, LEU162, LEU168, PRO163 residues.
(vi) One hydrophobic π- π stacking interaction.

The high number of noncovalent interactions between the complex **1** and N-protein was responsible for the high binding energy of compound **1**.

Compound **1** exhibited the cumulative best results in terms of inhibition of the major structural proteins. The binding constants were very high with respect to its other organometallic congeners and organic repurposed drugs. It also has a high inhibition potential against human Ca^{2+} channel protein with the binding energy of -13.74 kcal/mol and inhibition constant of 85.36 pM suggests it can also act as a Ca channel blocking agent. Thus, all these factors contribute to the regulation of cytokine storm and thereby decreasing the mortality rate of SARS-CoV-2 affected patients. Hence the compound **1** could be the potential candidate for in vitro or in vivo screening against SARS-CoV-2.

Compound 2 as the inhibitor of major proteins of SARS-CoV-2

Compound **2** is a ferrocene Compound with antiviral and antitumor properties that contains six rotatable bonds with six hydrogen bond acceptor atoms and four hydrogen bond donor atoms with a total polar surface area of 123.93 $Å^2$. Such structural properties potentially make compound **2** suitable for the inhibition of the viral proteins via the formation of several noncovalent bonds with the amino acid residues of the proteins. The ADME analysis revealed that compound **2** had a consensus $LogP_{o/w}$ of 1.91 and it was very much soluble in water. It also had low gastrointestinal absorption and blood brain barrier permeability with an additional property to inhibit CYP3A4 protein. Hence compound **2** can be used as an intravenous drug. The drug likeness analysis revealed no violations in terms of Lipinsky, Ghose, Veber, Egan, Muegge analysis, suggesting the acceptability of compound **2** as a drug.

Compound **2** inhibited the spike protein of SARS-CoV-2 with the binding constant of -6.67 kcal/mol and inhibition constant of 12.94 μM (Fig. S10, Table 2, 3). The interactions observed were

(i) Four hydrogen bonds with the ARG393, GLY354, and TYR505 residues of protein where compound **2** acts as acceptor and the residue act as donors.
(ii) Four hydrogen bonds with the ASP405 and ALA386 residues of protein where the compound 2 acts as a donor and the O atoms of the residues acts as acceptors.

(iii) Two hydrophobic alkyl-alkyl interactions with the ILE548, PRO620 residues.
(iv) One hydrophobic π-σ interaction with the ALA386 residue.
(v) One hydrophobic π- π stacking interaction.
(vi) Two electrostatic attractive interactions with the HIS34, ARG393 residues N atom and the Fe(II)-center with an effective distance of 5.02055 and 4.71662 Å, respectively.

Herein, although eight hydrogen bonding and two electrostatic interactions were present, there was a lack of other noncovalent interactions that attributes to the moderate binding energy.

The compound **2** bound to the RdRp protein with the binding energy of -6.84 kcal/mol and inhibition constant of 9.66 μM (Fig. S11, Table 2, 3). The interactions observed were

(i) Eight hydrogen bonds with the ARG553, LYS545, ARG553, ARG555, LYS621, and CYS622 residues of protein where compound **2** acts as acceptor and the residues acts as donors.
(ii) Two hydrogen bonds with the ASP623 residue of protein where complex **2** acts as a donor and the O atoms of the residues act as acceptors.
(iii) One electrostatic π-cation interaction with ARG555 residue.
(iv) One electrostatic attractive interaction with the ARG553 residue N atom and the Fe(II) center with an effective distance of 5.57274 Å.

Here also we observe an abundance of hydrogen bonds but a lack of other noncovalent interactions leading to the moderate binding energy.

Compound **2** strongly binds with the M_{pro} protein of SARS-CoV-2 with a binding energy of -10.18 kcal/mol and an inhibition constant of 0.03472 μM (Fig. 3, Table 2, 3). The interactions observed were-

(i) Six hydrogen bonds with the LYS5, ARG4, and GLN127 residues of protein where compound **2** acts as acceptor and the residues act as donors.
(ii) One carbon hydrogen bond with the ARG4 residue of protein where compound **2** acts as acceptor and the residue act as a donor.
(iii) One hydrophobic π- σ interaction with LYS5 residue.
(iv) Two electrostatic attractive interactions with the LYS5 residue N atoms and the Fe(II) center with an effective distance of 4.72347 and 4.74046 Å, respectively.

Although here also we observed a lower number of other noncovalent bonds an abundance of hydrogen bonds it was expected to exhibit moderate binding energy. But additionally, here we observe toe electrostatic attractive interactions involved by Fe(II) center with relatively low interaction distance. These bonds together attribute to the higher binding energy of Compound 2 towards M_{pro} protein of SARS-CoV-2.

Compound **2** binds with the N protein and results in total binding energy of -7.99 kcal/mol and inhibition constant of 1.38 μM (Fig. S12, Table 2, 3). The interactions responsible for the binding energy are the following -

(i) Five hydrogen bonds with the GLU137, GLN161, LEU162, GLY165, THR166 residues of protein where Compound 2 acts as acceptor and the residues act as donors.

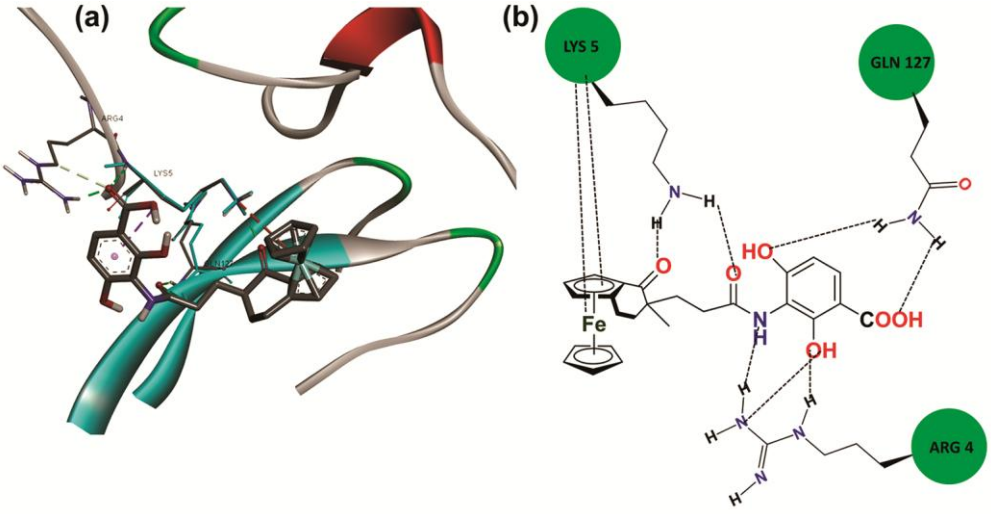

Fig. 3 — The best dock pose exhibiting non-covalent interactions between the compound **2** and the Mpro protein of SARS-CoV-2 and (b) Schematic representation of showing all the non-covalent interactions with LYS5, GLN127, ARG4 residues

(ii) Two hydrogen bonds with the THR166 and GLY70 residue of protein where compound **2** acts as a donor and the O atoms of the residues acts as acceptors.
(iii) One carbon hydrogen bond with the GLN161 residue of protein where Compound 2 acts as acceptor and the residue act as a donor.
(iv) One hydrophobic π-alkyl interaction with LEU162 residue.

Here the lack of other non-covalent interactions than hydrogen bonding and lack of electrostatic interactions reflects in the moderate binding energy.

Compound **2** can form strong hydrogen bonds with the protein residues but the lack of other non-covalent interactions resulted in the moderate binding energy of compound **2** with the proteins. But however, in the case of M_{pro} protein the compound **2** interacts with close electrostatic interactions by Fe(II) center, resulting in high binding energy. Hence compound **2** can be used to specifically target the M_{pro} protein of SARS-CoV-2 as it had higher binding energy towards it but had moderate binding energy towards the other three proteins.

Compound 3 as the inhibitor of major proteins of SARS-CoV-2

Compound **3** is also a ferrocene derivative with antiviral and antitumor properties. Compound **3** contains nine rotatable bonds with three hydrogen bond acceptor atoms and 1 hydrogen bond donor atom with a total polar surface area of 126.81 $Å^2$. This characteristic makes compound **3** suitable for orienting to the best pose of inhibiting the viral proteins via formation of several noncovalent bonds with the amino acid residues of the proteins. The ADME analysis reveals, Compound 3 had a consensus Log $P_{o/w}$ of 2.24 and it was moderately soluble in water. It also had high gastrointestinal absorption and blood brain barrier permeability with an additional property to inhibit CYP3A4 protein. Hence compound **3** can be used as oral, intravenous, intermuscular drug. The drug likeness analysis reveals no violations in terms Lipinsky, Ghose, Veber, Egan, Muegge analysis and all the data suggests the acceptability of compound **3** as a drug.

Compound **3** exhibits high binding energy of -9.38 kcal/mol with an inhibition constant of 0.13308 μM (Fig. 4, Table 2, 3) with the spike protein of SARS-CoV-2. The interactions observed were

(i) Two hydrogen bonds with the GLN76 residue of protein with the bond distance of 2.56 and 2.001 Å respectively where compound **3** acts as acceptor and the residues acts as donors.
(ii) Two hydrogen bonds with the GLU35 and GLU75 residue of protein where compound **3** acts as a donor and the O atoms of the residues act as acceptors with a bond length of 1.8242 and 3.26875 Å, respectively.

Although there was a lack of attractive electrostatic interactions and other noncovalent interactions the hydrogen bond that exists was of lower bond distance hence the formation of stronger bonds and leading to the higher binding energy.

Compound **3** at its most efficient binding mode exhibited binding energy of -8.91 kcal/mol with an inhibition constant of 0.29582 μM (Fig. S13, Table 2,

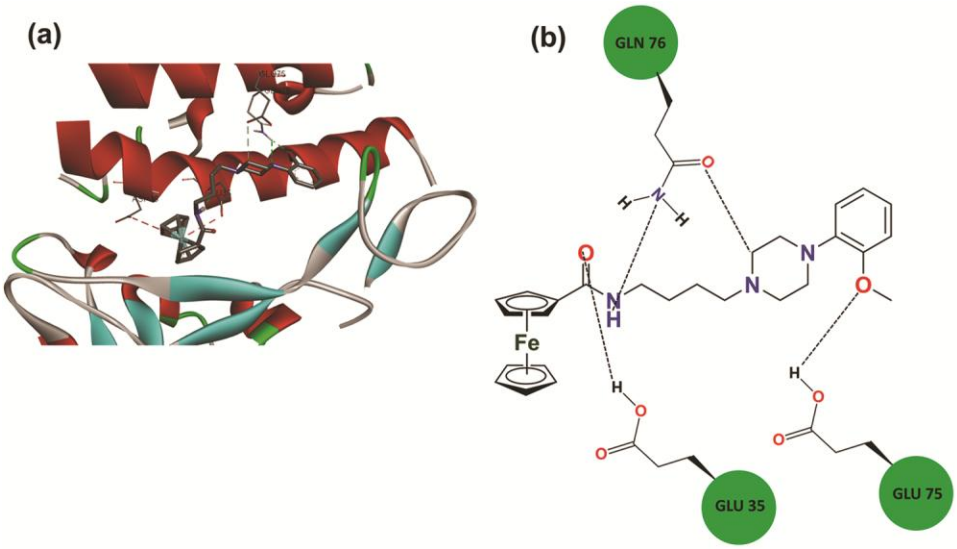

Fig. 4 — The best dock pose exhibiting non-covalent interactions between the compound **3** and the spike protein of SARS-CoV-2 and (b) Schematic representation of showing all the non-covalent interactions with GLN76, GLU35, GLU 75 residues

3) with the RdRp protein. The interactions observed were

(i) One hydrogen bond with the THR801 residues of protein where compound **3** acts as acceptor and the residues acts as donors.
(ii) Two hydrogen bonds with the GLU802 residue of protein where compound **3** acts as a donor and the O atoms of the residues act as acceptors.
(iii) Two hydrophobic T-shaped π- π interactions with TRP800 and HIS810 residue.

The T-shaped π- π interaction attributes and compensate for the lack of hydrogen bonding and other noncovalent interactions.

Compound **3** exhibits strong binding energy of -10.15 kcal/mol with an inhibition constant of 0.035 μM (Fig. S14, Table 2, 3) with M_{pro} protein of SARS-CoV-2. The interactions observed were-

(i) Two hydrogen bonds with the LYS173 and LEU287 residues of protein where compound **3** acts as acceptor and the residue act as donors.
(ii) Three hydrogen bonds with the ASP289, LEU287, and ALA285 residues of protein where Compound 3 acts as a donor and the O atoms of the residues act as acceptors.
(iii) Two carbon hydrogen bonds with the LEU287 and ALA285 residues of protein where compound **3** acts as acceptor and the residue acts as donors.
(iv) Two hydrophobic alkyl-alkyl interactions with the MET276, LEU287 residues.
(v) One hydrophobic π-σ interaction with the LEU272 residue.
(vi) One hydrophobic π- alkyl interaction with LEU287 residue.
(vii) Three electrostatic attractive interactions with the LYS5 and LYS137 residue N atom and the Fe(II) center with an effective distance of 4.8-5.3 Å.

The short attractive electrostatic interactions and the presence of hydrogen bonds along with noncovalent interactions attribute to the high binding energy.

Compound **3** exhibits moderate binding energy of -7.14 kcal/mol with an inhibition constant of 5.87 μM (Fig. S15, Table 2, 3) with the N protein. The interactions observed were

(i) Two hydrogen bonds with the GLN71 and GLN84 residues of protein where compound **3** acts as acceptor and the residue act as donors.
(ii) One carbon hydrogen bond with the GLY70 residue of protein where compound **3** acts as acceptor and the residue acts as donors.
(iii) Three hydrophobic π- alkyl interactions with LEU160, LEU162 and LEU168 residues.

The lack of non-covalent interaction attributes to the moderate binding energy compared to the organic congeners.

Compound **3** due to its low no of hydrogen bond donor and acceptor atom, cannot form many interactions but however due to its high flexibility it can orient itself as such the bond distance become low for the interactions and as a result, stronger bonds were formed leading to the higher binding energy. Compound **3** exhibits a very good binding affinity towards the spike protein, RdRp protein, and M_{pro} protein with the exception of only N protein. But the binding energy with N protein was comparable to that of organic congeners, thereby compound **3** can be a potential candidate as a drug against SARS-CoV-2.

Compound 4 as the inhibitor of major proteins of SARS-CoV-2

The last pick compound **4** is also a ferrocene Compound with antiviral and antitumor properties. Compound **4** contains seven rotatable bonds with two hydrogen bond acceptor atoms and one hydrogen bond donor atom with a total polar surface area of 49.41 $Å^2$. These characteristic makes Compound **4** suitable for orienting to the best pose of inhibiting the viral proteins via formation of several noncovalent bonds with the amino acid residues of the proteins. The ADME analysis reveals, compound **4** had a consensus Log $P_{o/w}$ of 2.17 and it was soluble in water. It also had high gastrointestinal absorption and blood brain barrier permeability with an additional property to inhibit CYP3A4 protein. Hence compound **4** can be used as an oral, intervenous, intermuscular drug. The drug likeness analysis reveals no violations in terms Lipinsky, Ghose, Veber, Egan, Muegge analysis, suggests the acceptability of Compound 4 as a drug.

Compound **4** exhibits moderate binding energy of -7.09 kcal/mol with an inhibition constant of 6.4 μM (Fig. S16, Table 2, 3) with the spike protein of SARS-CoV-2. The interactions observed were

(i) Three hydrogen bonds with the HIS34, ASN33, and GLU37 residues of protein where compound **4** acts as a donor and the O atoms of the residues act as acceptors.

(ii) Two carbon hydrogen bonds with the HIS34 and GLU37 residues of protein where compound **4** acts as acceptor and the residue act as donors.
(iii) One hydrophobic π-σ interaction with the HIS34 residue.
(iv) Two electrostatic attractive interactions with the LYS353 and LYS403 residue N atom and the Fe(II) center with an effective distance of 4.3-5.2 Å.

The lack of hydrogen bond donor and acceptor atom leads to less amount of hydrogen bonding interactions and thereby leading to moderate binding energy.

Compound **4** binds strongly with RdRp protein of SARS-CoV-2 with a binding energy of -8.59 kcal/mol with an inhibition constant of 0.50219 μM (Fig. S17, Table 2, 3). The interactions observed were

(i) One hydrogen bond with the LEU473 residue of protein where compound **4** acts as acceptor and the residue act as donor.
(ii) One hydrogen bond with the PHE429 residue of protein where compound **4** acts as a donor and the O atom of the residues acts as acceptors.
(iii) One carbon hydrogen bond with the SER4 residues of protein where compound **4** acts as acceptor and the residue act as donors.
(iv) Six hydrophobic alkyl-alkyl interactions with the LEU437, LYS7, LYS438, CYS8 residues.
(v) Three hydrophobic π- alkyl interactions with PHE440 and PHE843 residues.
(vi) One electrostatic attractive interaction with the SER1 residue N atom and the Fe(II) center with an effective distance of 4.82123 Å.

The presence of strong electrostatic attractive interactions and other non-covalent interactions with hydrogen bonding attributes to the higher binding energy of the compound.

Compound **4** binds strongly with M_{pro} protein of SARS-CoV-2 with a binding energy of -9.46 kcal/mol with an inhibition constant of 0.11622 μM (Fig. S18, Table 2, 3). The interactions observed were-

(i) Four hydrogen bonds with the LYS5 and GLN127 residues of protein where compound **4** acts as acceptor and the residue act as donor.
(ii) Two hydrogen bonds with the GLN127 residue of protein where compound **4** acts as a donor and the O atom of the residues act as acceptors.
(iii) One carbon hydrogen bond with the SER4 residues of protein where compound **4** acts as acceptor and the residue act as donors.
(iv) Two hydrophobic alkyl-alkyl interactions with the LEU5 residue.
(v) Two electrostatic attractive interactions with the LYS5 residue N atom and the Fe(II) center with an effective distance of 5.17-5.22 Å.

The presence of strong electrostatic attractive interactions and other non-covalent interactions with hydrogen bonding attributes to the higher binding energy of the compound.

Compound **4** exhibits moderate binding energy of -7.92 kcal/mol with an inhibition constant of 1.57 μM (Fig. S19, Table 2, 3) with the N protein of SARS-CoV-2. The interactions observed were

(i) One hydrogen bond with the GLU137 residue of protein where compound **4** acts as acceptor and the residue act as a donor.
(ii) Three carbon hydrogen bonds with the THR166 residues of protein where compound **4** acts as acceptor and the residue act as donors.
(iii) Two hydrophobic alkyl-alkyl interactions with the PRO163 and LEU168 residue.

The lack of hydrogen bond donor and acceptor atom leads to less amount of hydrogen bonding interactions and thereby leading to moderate binding energy.

Due to the lesser amount of hydrogen bond donor and acceptor atoms were present in Compound **4** it generally binds with structural proteins vial formation of a few numbers of hydrogen bonds and non-covalent bonds. But it can strongly bind with the RdRp protein and M_{pro} protein vial formation of electrostatic attractive interactions by the influence of Fe(II) center. This emerges compound **4** as a better drug for SARS-CoV-2 in comparison to the organic repurposed drugs.

The molecular docking calculation of ferrocene-based compounds in the major viral proteins of SARS-CoV-2 revealed that selected compounds are excellent inhibitors of all the viral proteins. These compounds exhibit binding energy in the range of -7 to -13 kcal/mol which is considered as high in terms of inhibition properties. But among these results, compound **1** exhibited the highest binding energies (-8.8 to -13.12 kcal/mol) with all the viral proteins. Hence compound **1** raises the scope of further investigation into the multi targeting aspect to prevent other cascading situations which occur in the COVID-19 patients.

Compound 1 as Ca^{2+} ion channel blocker

The increased intracellular Ca^{2+} ion concentration of SARS-CoV-2 patients has been a major concern in

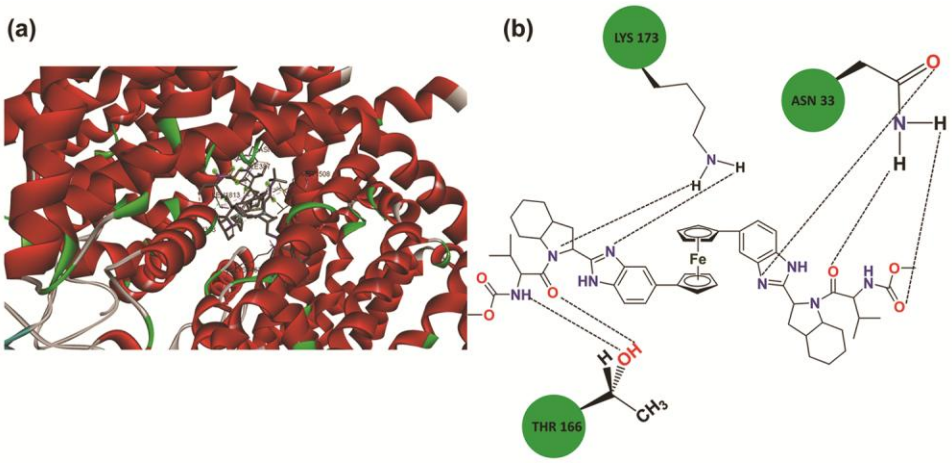

Fig. 5 — The best dock pose exhibiting non-covalent interactions between the compound **1** and the human Ca^{2+} channel protein and (b) Schematic representation of showing all the non-covalent interactions with THR166, ASN33, LYS173 residues

respect to the mortality rates as it can alter the signal transaction pathways and trigger a series of biochemical cascades that eventually leads to over inflammation and multiorgan failure. Therefore, blocking of human Ca^{2+}-channel could be an attractive strategy to prevent ARDS and death to the COVID-19 infected patient. So herein we have studied the molecular docking of compound **1** against human Ca^{2+}-channel protein and observed that it has a significantly high binding energy of -13.74 kcal/mol and an inhibition constant of 85.36 pM (Fig. 5, Table 2, 3) against the said protein. Hence our compound 1 has excellent potential to act as a drug in the treatment of SARS-CoV-2. The high binding energy is attributed to the following interactions-

(i) Seven hydrogen bonds with the LYS1462, ASN952, MET1508, THR921, and ASN388 residues of protein where compound **1** acts as acceptor and the residue act as a donor.

(ii) Five hydrophobic alkyl-alkyl interactions with the ILE387, VAL1393, MET1508, LEU1813 residues.

Compound **1** shows excellent binding and inhibition properties against human Ca^{2+} channel protein and it is a potential candidate for inhibiting SARS-CoV-2 viral proteins and inhibitor of signalling transaction cascade processes there by it can reduce the mortality rate in SARS-CoV-2 patients.

Conclusions

The outbreak of SARS-CoV-2 virus has resulted in a worldwide health crisis in the last two years with a very high infection rate and it caused a large number of mortalities. Herein, we implemented SAR based approach in which the selected anticancer Ferrocene based compounds inhibited the major viral proteins like spike protein, RdRp protein, M_{pro} protein, and N protein, and also human Ca^{2+}-channel proteins as revealed from the molecular docking studies in silico. Compounds **1-4** exhibited remarkable binding affinity towards the major viral proteins of the COVID-19 with the binding energies >9.0 kcal/mol (inhibition constant: <0.2 mM). Among the selected compounds, compound **1** exhibited the highest binding energies against all the viral proteins. Hence compound **1** was also investigated as the inhibitor of the human Ca^{2+} channel which resulted in the binding energy -13.74 kcal/mol (inhibition constant: 85.36 pM). The overall computational studies projected ferrocene derivatives as the strategic tools for combination therapy to the severe virus-affected patients in their respiratory distress condition and could be the alternative and attractive therapeutic solution to the pandemic COVID-19.

Supplementary Data

Supplementary information is available in the website http://nopr.niscair.res.in/handle/123456789/58776.

Acknowledgments

We sincerely thank the Board of Research in Nuclear Science (BRNS), Mumbai (37(2)/14/18/2017-BRNS) and Science and Engineering Research Board (SERB) (CRG/2021/004337) for financial support, MHRD India for scholarship support, and NIT Manipur for providing infrastructure. We sincerely thank Prof. Sukesh Mukherjee, AIIMS Bhopal, and Dr. Amit Kunwar, BARC, Mumbai for

initial discussions. We also thank TEQIP-III (NPIU), NIT Manipur for providing computational infrastructure that facilitated our in-silico studies.

References

1 who.int/emergencies/diseases/novel-coronavirus-2019/situation-reports.
2 Petrosillo N, Viceconte G, Ergonul O, Ippolito G & Petersen E, *Clin Microbiol Infect*, 26 (2020) 729.
3 Hu B, Guo H, Zhou P & Shi Z L, *Nat Rev Microbiol*, 19 (2021) 141.
4 Abdelrahman Z, Li M & Wang X, *Front Immunol*, 11 (2021)1.
5 Rothan H A & Byrareddy S N, *J Autoimmun*, 109 (2020) 102433.
6 Harrison A G, Lin T & Wang P, *Trends Immunol*, 41 (2020) 1.
7 Li X, Geng M, Peng Y, Meng L & Lu S, *J Pharm Anal*, 10 (2020) 102.
8 https://www.who.int/docs/default-source/coronaviruse/key-messages-and-actions-for-covid-19-prevention-and-control-in-schools-march-2020.
9 Krammer F, *Nature*, 586 (2020) 516.
10 Yadav T, Srivastava N, Mishra G, Dhama K, Kumar S, Puri B & Saxena S K, *Hum Vaccin Immunother*, 16 (2020) 2905.
11 Rawat K, Kumari P & Saha L, *Eur J Pharmacol*, 892 (2021) 173751.
12 Lundstrom K, *Front Genome Ed*, 2 (2020) 579297.
13 Harvey W T, Carabelli A M, Jackson B, et al., *Nat Rev Microbiol*, 19 (2021) 409.
14 https://www.who.int/en/activities/tracking-SARS-CoV-2-variants.
15 https://www.fda.gov/medical-devices/coronavirus-covid-19-and-medical-devices/sars-cov-2-viral-mutations-impact-covid-19-tests.
16 Costanzo M, De Giglio M A R & Roviello G N, *Curr Med Chem*, 27 (2020) 4536.
17 Drożdżal S, Rosik J, Lechowicz K, Machaj F, Kotfis K, Ghavami S & Łos M J, *Drug Resist Updat*, 53 (2020) Article 100719.
18 https://www.fda.gov/news-events/press-announcements/fda-approves-first-treatment-covid-19.
19 Weisberg E, Parent A, Yang P L, Sattler M, Liu Q, Liu Q, Wang J, Meng C, Buhrlage S J, Gray N & Griffin J D, *Pharm Res*, 37 (2020) 167.
20 Misra S, Nath M, Hadda V & Vibha D, *medRxiv*, 1 (2020) 1.
21 Singh T U, Parida S, Lingaraju M C, Kesavan M, Kumar D & Singh R K, *Pharmacol Rep*, 72 (2020) 1479.
22 Huang Y, Yang C, Xu X F, Xu W & Liu S W, *Acta Pharmacol Sin*, 41 (2020) 1141.
23 V'kovski P, Kratzel A, Steiner S, Stalder H & Thiel V, *Nat Rev Microbiol*, 19 (2021) 155.
24 Venkatagopalan P, Daskalova S M, Lopez L A, Dolezal K A & Hogue B G, *Virology*, 478 (2015) 75.
25 Cao Y, Yang R, Lee I, Zhang W, Sun J, Wang W & Meng X, *Protein Sci*, 30 (2021) 1114.
26 Mandala V S, McKay M J, Shcherbakov A A, Dregni A J, Kolocouris A & Hong M, *Nat Struct Mol Biol*, 27 (2020) 1202.
27 Danta C C, *ACS Pharmacol Transl Sci*, 4 (2021) 400.
28 Lee J W, Ko J, Ju C & Eltzschig H K, *Exp Mol Med*, 51 (2019) 1.
29 Rothan H A, Stone S, Natekar J, Kumari P, Arora K & Kumar M, *Virology*, 547 (2020) 7.
30 Ornelas C, *New J Chem*, 35 (2011) 1973.
31 Larik F A, Saeed A, Fattah T A, Muqadar U & Channar P A, *Appl Organomet Chem*, 31 (2016) e3664.
32 Santos M M, Bastos P, Catela I, Zalewska K & Branco L C, *Mini Rev Med Chem*, 17 (2017) 771.
33 Peter S & Aderibigbe B A, *Molecules*, 24 (2019) 3604.
34 Patra M & Gasser G, *Nat Rev Chem*, 1 (2017) Article 0066.
35 Xiao J, Sun Z, Kong F & Gao F, *Eur J Med Chem*, 185 (2020) 111791.
36 Pal M, Musib D & Roy M, *New J Chem*, 45 (2021) 1924.
37 Pal M, Musib D, Zade A J, Chowdhury N & Roy M, *ChemistrySelect*, 6 (2021) 7429.
38 Sethi A, Joshi K, Sasikala K & Alvala M, *Molecular docking in modern drug discovery: principles and recent applications In drug discovery and development-new advances*, (IntechOpen, London) 2019
39 Walls A C, Park Y J, Tortorici M A, Wall A, McGuire A T & Veesler D, *Cell*, 181 (2020) 281.
40 Gao Y, Yan L, Huang Y, Liu F, Zhao Y, Cao L, Wang T, Sun Q, Ming Z, Zhang L, Ge J, Zheng L, Zhang Y, Wang H, Zhu Y, Zhu C, Hu T, Hua T, Zhang B, Yang X, Li J, Yang H, Liu Z, Xu W, Guddat L W, Wang Q, Lou Z & Rao Z, *Science*, 368 (2020) 779.
41 Kang S, Yang M, Hong Z, Zhang L, Huang Z, Chen X, He S, Zhou Z, Zhou Z, Chen Q, Yan Y, Zhang C, Shan H & Chen S, *Acta Pharm Sin B*, 10 (2020) 1228.
42 Jin Z, Du X, Xu Y, Deng Y, Liu M, Zhao Y, Zhang B, Li X, Zhang L, Peng C, Duan Y, Yu J, Wang L, Yang K, Liu F, Jiang R, Yang X, You T, Liu X, Yang X, Bai F, Liu H, Liu X, Guddat L W, Xu W, Xiao G, Qin C, Shi Z, Jiang H, Rao Z & Yang H, *Nature*, 582 (2020) 289.
43 (a) Gaussian 09, Revision C.01, Frisch M J, Trucks G W, Schlegel H B, Scuseria G E, Robb M A, Cheeseman J R, Scalmani G, Barone V, Petersson G A, Nakatsuji H, Li X, Caricato M, Marenich A V, Bloino J, Janesko B G, Gomperts R, Mennucci B, Hratchian H P, Ortiz J V, Izmaylov A F, Sonnenberg J L, Williams-Young D, Ding F, Lipparini F, Egidi F, Goings, J, Peng B, Petrone A, Henderson T, Ranasinghe D, Zakrzewski V G, Gao J, Rega N, Zheng G, Liang W, Hada M, Ehara M, Toyota K, Fukuda R, Hasegawa J, Ishida M, Nakajima T, Honda Y, Kitao O, Nakai H, Vreven T, Throssell K, Montgomery J A, Jr Peralta J E, Ogliaro F, Bearpark M J, Heyd J J, Brothers E N, Kudin K N, Staroverov V N, Keith T A, Kobayashi R, Normand J, Raghavachari K, Rendell A P, Burant J C, Iyengar S S, Tomasi J, Cossi M, Millam J M, Klene M, Adamo C, Cammi R, Ochterski J W, Martin R L, Morokuma K, Farkas O, Foresman J B, Fox D J, Gaussian Inc. Wallingford CT 2016; (b) Barolo C, Nazeeruddin Md K, Fantacci S, Di Censo D, Comte P, Liska P, Viscardi G, Quagliotto P, De Angelis F, Ito S & Grätzel M, *Inorg Chem*, 45 (2006) 4642.
44 http://www.swissadme.ch
45 Morris G M, Huey R, Lindstrom W, Sanner M F, Belew R K, Goodsell D S & Olson A J, *J Comput Chem*, 30 (2009) 2785.
46 BIOVIA, Dassault Systèmes, Discovery Studio Visualizer 09, San Diego: Dassault Systèmes, 2020.